Impact of CIR processing for UWB radar distance estimation with the DW1000 transceiver

Ben Van Herbruggen*, Stijn Luchie*, Rafael Berkvens†,Jaron Fontaine* and Eli De Poorter*
*INTEC-IDLab, Ghent University-IMEC, Ghent, Belgium
†IDLab, University of Antwerp-IMEC, Antwerp, Belgium
Email: ben.vanherbruggen@ugent.be

***Abstract*—Automatic distance detection is essential for industrial safety processes, allowing detection of persons in unsafe zones, detecting obstacles nearby autonomous vehicles, etc. ultra-wideband (UWB) radar is a recent upcoming technology that is suitable for low-cost, device-free distance estimations to persons and obstacles. The excellent time properties of UWB allow the detection of distinct propagation paths from sender to receiver and reflecting objects. Currently, existing work utilizes dedicated UWB radar hardware. This paper focuses on off-the-shelf DW1000 UWB transceivers which have lower cost but also lower time resolution of the received channel impulse response (CIR). We analyze three data processing methods (ICIR, UCIR, and ACIR). Next, we analyze two distance estimation approaches in a realistic industrial environment: a mean based and a variance based. We demonstrate that selecting the best combination of data processing and distance estimator is crucial, allowing the detection of metal objects up to 900 cm with a mean accuracy of 9 cm, or the detection of persons with a mean absolute error of only 44 cm.**

***Index Terms*—ultra-wideband, UWB, radar, localization, distance estimation, object detection**

I. Introduction

Industry 4.0 has known a rapid progression with many new IoT technologies being deployed [1]. One of the existing considerations inside factories is safety and how to implement this. Such safety applications include the following use cases: collision detection and prevention between autonomous guided vehicle (AGV) and or personnel/visitors, intrusion detection, proximity detection [2], [3], etc. Currently, the main technologies for detecting objects are lidar, camera-based, and high-frequency radar technologies, but these technologies are expensive, difficult to calibrate, or not privacy-conscious. Another possibility is the use of radio frequency communication links for detecting objects. When two or more devices are fixed and wirelessly communicating with each other, the room can be sensed at the same time. This simultaneous communication and sensing could improve safety in Industry 4.0 plants and at the same time provide reliable communication.

UWB technology has emerged as a promising solution for object detection and proximity sensing. Unlike other wireless technologies such as BLE or Wi-Fi, UWB technology operates with a much higher bandwidth (0.5 to 2.5 GHz) which allows for precise time-of-flight measurements and accurate distance calculations. One of the key advantages of UWB technology is its ability to accurately detect and locate objects in real-time, even in environments with high levels of reflections with battery-constrained devices [4]. The technology is considered non-intrusive due to its low power spectral density. Recent scientific work focused mainly on manufacturing use cases where UWB is applied for collision detection and asset tracking [4] where fixed infrastructure is used to communicate and track assets that are equipped with active UWB nodes. However, attaching a UWB tag to each object and person is often not feasible, nor cost-efficient. Instead, UWB radar applications detect obstacles or persons even when they are not equipped with UWB tags. In these radar applications a representation of the propagation channel of the UWB pulses, the CIR, can be exploited. UWB can penetrate walls and objects that obstruct visual sight [5]. In [6], UWB is used for through-the-wall detection of humans. Different decomposition techniques are tested on UWB radar units with wooden, brick, and concrete walls. Other short-range UWB radar applications include vital sign monitoring [7], room occupancy detection [8], seat belt reminder systems [9], etc.

The above scientific publications use custom-built UWB radar setups, rather than cheaper, commercial off-the-shelf (COTS) radio chips. As such, it is not clear how well such solutions would scale towards COTS frequently used transceivers. The contributions in this paper that extend the current state-of-the-art in UWB radar are:

- This paper is the first to experimentally evaluate the accuracy of the popular DW1000 for object and person distance detection in a realistic industrial environment.
- Three different CIR data processing techniques are described and their impact on the accuracy of object detection is discussed.
- Two different object detection algorithms are presented and evaluated.

The remainder of this paper is structured as follows: Section II discusses the technical background of UWB radar and existing work. In Section III the data collection campaign is discussed. The algorithms used for object detection are proposed in Section IV. Section V discusses the results of bi-static object detection. Section VI concludes the paper.

This research is partially funded by Research Foundation - Flanders (FWO) PESSO project under grant number: G018522N.

II. Technical Background

Radar configurations typically include at least 2 antennas. One antenna is used for sending the UWB pulse while the second one is used to receive the pulse. Depending on the location and number of receivers, three different categories can be distinguished. If both transmitting and receiving antennas are on the same device, it's called mono-static radar. In bi-static radar, the sender and receiver will be separated. The transmitter sends a packet from one location which is reflected and collected by the receiver at a second location. When multiple receivers are used, it's multi-static radar. Fig. 1 illustrates the difference between the three main radar techniques.

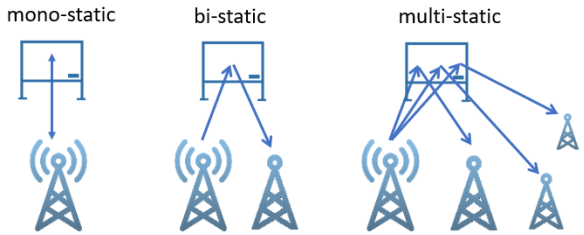

Fig. 1. Different configurations: mono-static: transmitter and receiver are at the same location, bi-static: transmitter and receiver are separated, and multi-static: multiple receivers at different locations are used.

Ultra-wideband (UWB) multi-static radar has been used for device-free person tracking [10]–[12]. However, these solutions require the installation of multiple devices at different locations across a room, which poses complex deployment and synchronization challenges. Currently, most use cases for multi-static UWB radar focus on the tracking of dynamic assets. In [10] the authors placed three DW1000-based receivers in a triangle, and propose a method to deduce the multipath components (MPC) from the CIRs. Together with the environmental topology, they are able to track persons with 50% of the points localized within 1.63 m. A second approach combines UWB multi-static radar with radio tomographic imaging for UWB, which resulted in a localization error of 0.64 m. A similar approach is used in [11], [12] where the setup consists of a square with 4 DW1000-based devices with high update rates. Localization accuracies of less than 30 cm are reported. In contrast to the previous publications, we assume a distributed setup will not be feasible in industrial applications, due to safety protocols and power supply requirements. Instead, our work assumes a setup whereby all anchors are collinear and close to each other, representing for example an installation close to the wall.

The channel impulse response (CIR) is the most used attribute for UWB radar applications as it contains information about the environment. Due to the excellent time resolution of UWB signals [13], [14], paths with different distances are clearly separated in time. Fig. 2 shows different CIRs in the same environment where each time an object is placed at different distances from the radar nodes. The CIR is reported by the DW1000 as IQ samples, but for distance estimation, the amplitude in the time domain contains the most useful information. The CIR can be represented by the superposition of the arriving pulses with each a specific delay and attenuation (Equation 1).

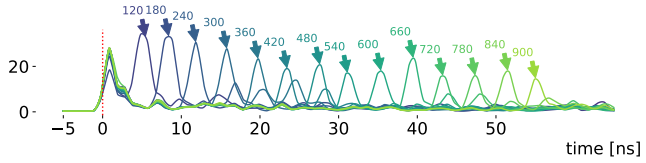

Fig. 2. CIRs captured when the distance to the same reflecting object is varying. The further the object is, the more path loss occurs at the reflected path and the lower the peak of the reflected signal becomes. The distance of the object is annotated to the corresponding peak in the CIR.

$$CIR(t) = \sum_k a_k * \delta(t - \tau_k) + n_k, \tag{1}$$

where the receiving pulse k has an amplitude a_k, time delay τ_k and noise n_k. In ideal conditions, the direct path and the reflection on the targeted object will be the only peaks in the CIR. However, all static objects, often referred to as clutter, that reflect will add extra peaks in the CIR. Furthermore, the noise n_k in the channel is dependent on the environment of the data collection, the chosen UWB PHY parameters, antenna gains, and interfering technologies. It can be modeled as Gaussian noise. Due to the different path lengths that reflected pulses travel, extra peaks in the CIR will be visible. In [15], these so-called MPCs are modeled in the presence of a person walking a path. Based on the specific time delay of a pulse in the channel impulse response, the extra length of the reflected path is determined. Each ellipse, with the transmitter and receiver as focal points, in Fig. 3 depicts places where reflections have an identical time delay and these points are therefore not distinguishable in the CIR. The number of samples after the first path determines the maximal additional time delay a reflection pulse can have: collecting more samples increases the detection range. If 25 samples are collected after the first path and every sample has a precision of 1.0016 ns, then the maximal extra allowed path length is $25 \times 1.0016ns \times c = 7.5m$. However, collecting more CIR samples impacts the complexity and reduces the maximum update rate.

III. Measurement and Data Collection

This section will discuss the testing environments and the objects that are used for object detection.

A. Data collection environment

The data collection campaign has been organized in a controlled lab environment of the IDLab research group at Ghent University (Fig. 4). The industrial internet of things (IIoT) lab [16] is equipped with an accurate mm-level ground truth motion capturing (MOCAP) system. The UWB data is collected with the Wi-Pos UWB system [13], a platform developed for research data collection with a wireless long-range sub-GHz backbone combined with UWB ranging based

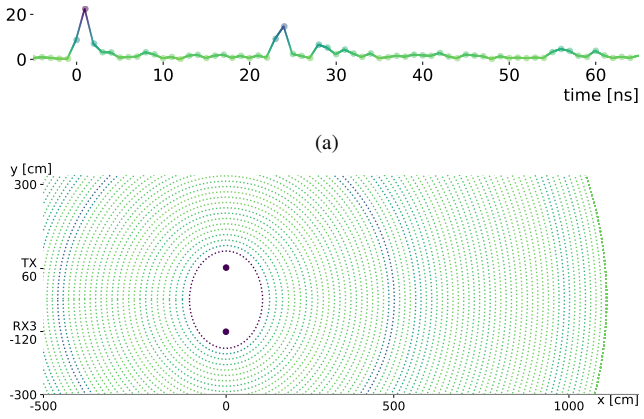

Fig. 3. All pulses that reflect on a place on the same ellipse, will result in a peak in the corresponding CIR.

on the DW1000, as shown in Fig. 4a. The platform consists of the COTS Zolertia RE-Mote and a shield containing the DW1000 with an SMA connector to connect different antennas. For the data collection, omnidirectional antennas are used. A software stack is implemented on the RE-Mote to execute a TDMA-based medium access control layer to control the scheduling of the UWB packets. The long-range backbone for communication and TDMA synchronization enables the devices to run on battery power for multiple days. The UWB is configured to use channel 7 with a center frequency of 6489.6 MHz and a receiving bandwidth of 900 MHz. A short preamble of 128 symbols is used at the suggested TX power (7.5 dB) from the DW1000 user manual [17]. The bitrate for the measurements is 850 kbps and a pulse repetition frequency (PRF) of 64 MHz is used. Finally, the CIRs are collected with an update rate of 35 Hz. Four UWB nodes are positioned in a straight line. Each node is positioned approximately 60 cm away from each other. The most right one is chosen to be the transmitting device. The other three devices act as receivers. Fig. 4b depicts this setup.

B. Test objects

Three different objects and one person are used as test subjects and are placed every 60 cm between 1.2 and 9.0 m. The objects are i) **a whiteboard**, made of a smooth, flat surface reflecting material, typically used for writing with dry-erase markers. The used whiteboard has dimensions of 118 cm by 199 cm. ii) **A large TV**, a rectangular-shaped object typically made of multiple materials such as glass, metal, and plastic. The TV has a height of 87 cm and a width of 150 cm. iii) As the third object **a smaller metal box** of 34 by 58 cm is used. iv) **A person**, who absorbs and reflects RF signals as a living organism. In contrast to metal objects, reflections from persons may not be as strong and can be affected by small movements in breathing and body position stability. For this study, we used a male person of 1.9 m.

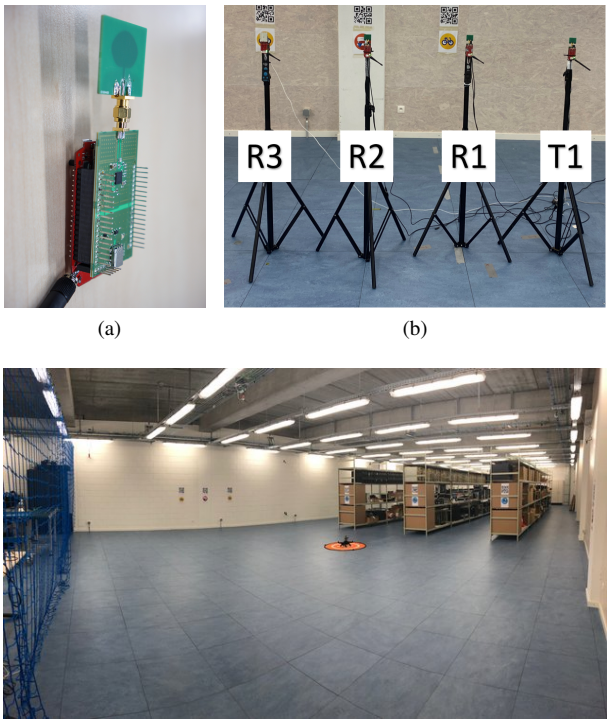

Fig. 4. The data collection is done with a bi-static radar setup. (a) The Wi-Pos hardware platform with DW1000 transceiver [13] is used. (b) The three receivers and one transmitter are on one line to analyze the effect of distance between sender and receiver. (c) The data is collected in the open area of an industrial environment.

C. Determination of ground truth

To objectively compare the influence of the distance between the transmitter and receiver, we will take the distance of the object to the line crossing transmitter and receiver. To calculate this ground truth distance, both the UWB devices and the object are measured with the mm-accurate MOCAP system. After detecting the important peak in the CIR, this corresponding extra path length needs to be converted to this ground truth distance. The definition of the ground truth is shown in Fig. 5

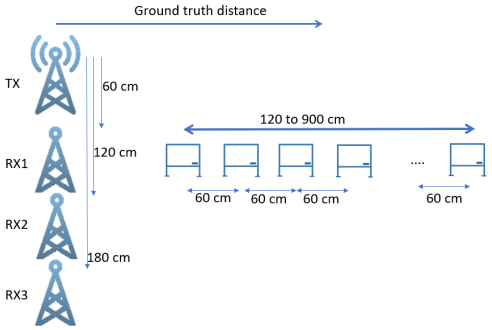

Fig. 5. Schematic design of the setup and the definition of the ground truth.

IV. Object detection algorithm

To detect objects and sense changes in the room, CIRs are collected at 35Hz both in the empty room (the background CIR) and in the presence of obstacles (obstacle CIR). These sets of CIRs contain information on the reflections of the transmitted pulses on the room contours (wall, floor, ceiling), the furniture, and the obstacles.

A. CIR data processing techniques

The noise present on the channel n_k influences the CIR. The DW1000 reports the CIR with a time granularity of one IQ sample every 1 ns. However, internally in the receiver, the sample of the first path (fp_{index}) is calculated and reported at a much higher resolution of 15.65 ps which corresponds to 1/64th of the precision of a CIR sample. As such, peaks in the CIR (which are the most interesting for radar) have a much lower time resolution than the first path index. We evaluate three different techniques to process the CIRs. After this data processing step, the m last collected instances can be combined towards a single low-noise representation with the object distance estimation algorithms. Combining more CIRs will simplify object detection but lengthens data collection time which leads to larger response times for new objects. The three data processing techniques are presented in Fig. 6.

*1) **Integer channel impulse response (ICIR)**:* is a method of aligning CIRs (Channel Impulse Responses) in time using the integer part of the reported first path. The CIR is adjusted so that it is centered around the sample just before the first path ($floor(fp_{index})$), which is considered as time 0 after the adjustment. The purpose of ICIR is not to improve spatial resolution but to establish a common time reference for the CIRs. This approach has a relatively simple computational process, but the alignment may still have some degree of noise.

*2) **Upsampling channel impulse response (UCIR)**:* the CIR time resolution is enhanced by a factor 64 by applying a quadratic interpolation filter, thereby increasing the granularity to match that of the reported first path. Subsequently, the CIRs are aligned with each other using a highly accurate time resolution of 15.65 ps. In the aligned CIRs, the reported first path (fp_{index}) is positioned at time 0. Compared to ICIR, UCIR provides improved alignment of the CIRs, but this increased alignment precision comes at the cost of higher computational complexity without necessarily adding additional information.

*3) **Accumulation channel impulse response (ACIR)**:* method shares similarities with ICIR in terms of aligning the CIRs using the integer part of the first path index. However, ACIR introduces additional steps to further refine the alignment process. Each CIR is assigned to a specific bin based on the fractional part of the first path index. Within each bin, multiple CIRs are averaged together. If there are any empty bins, they are interpolated to ensure a complete alignment. The data from these bins is merged to generate a CIR that reflects a higher level of spatial detail equal to the temporal resolution of the fractional part of the first path index. Additionally, a smoothing technique can be optionally applied to further enhance the quality of the aligned CIRs. The ACIR method has been utilized in research papers such as [11] and [2].

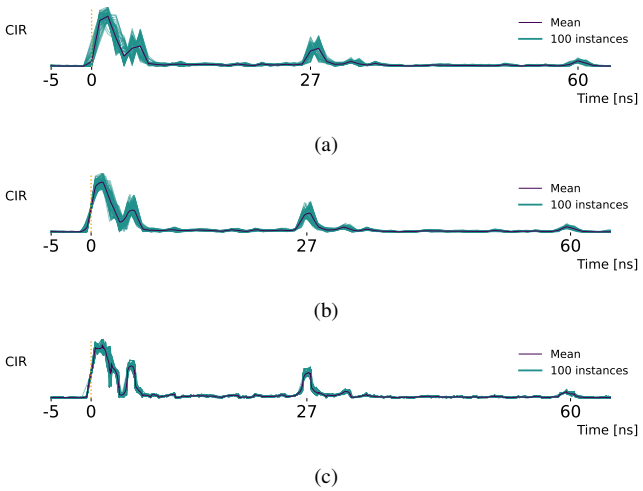

Fig. 6. Multiple collected CIRs are aligned using three different data processing techniques. a) using ICIR, individuals are still deviating from their mean value. b) in UCIR the alignment is better but the CIR does not go to zero between the first and second peak while in c) ACIR these peaks are clearly separated.

B. Object distance estimation algorithms

Next, the aligned CIRs are combined and the distance to objects is estimated using on the below proposed techniques. The bi-static mean algorithm (BMA) algorithm tries to limit the influence of the noise on the samples of the CIR for detection, while the bi-static standard deviation algorithm (BSDA) exploits information that is incorporated into the variation on samples. For multi-static person tracking using the variance in the CIR samples has proven to give good results [11], [12], but this has not yet been validated on static object detection with bi-static radar configurations.

*1) **Bi-static mean algorithm (BMA)**:* An average CIR is calculated for both the background collection and the CIR when the object is present by taking the mean value of every sample over all CIRs. The RF character of the room will be mainly changed by the new object in the room. As such, the CIR shows a clear extra peak when a new reflection arrives a few nanoseconds after the direct path. Longer paths suffer from more path loss effects and result in smaller peaks. Similar to objects introducing new peaks, peaks can be lower when objects are blocking other paths in the room. To find the region with the highest changes, the background average CIR (without the object) is subtracted from the average CIR with the object. By searching for the highest peak in this difference, the new peak and corresponding object can be estimated.

*2) **Bi-static standard deviation algorithm (BSDA)**:* The second detection algorithm takes the standard deviation per sample to detect and estimate the objects in the room. Similar to BMA, a background variant and a variant when sensing are subtracted from each other. The distance of the object is then estimated by the highest peak in this difference. When

the surface of the object is scattering the reflecting waves differently than the background environment this is noticeable in the CIR by observing higher variation in the arriving CIR. And in addition, vibrations of different objects, including the person, also increase variability in consecutive CIRs.

V. Bi-static radar Results

In this section we present the distance estimation accuracies estimated by the proposed algorithms. First, the influence of the data processing is discussed, followed by the influence of the distance between transmitter and receiver, the different objects, the detection latency and a more detailed discussion on the person detection. Each specific combination of testing parameters has been executed 100 times to cancel out Monte Carlo effects of the chosen CIRs for object detection.

A. Influence of the data processing method

Three different data processing techniques are applied on one second of data (35 samples) before running the two detection algorithms. The cumulative distribution functions (cdfs) of these data processing object detection for all objects and all receivers are given in Fig. 7. The ICIR has the lowest mean accuracy (85 cm for BMA and 82 cm for BSDA). The ACIR reports similar results for BMA (85 cm), but performs worse with the BSDA algorithm (137 cm) as this representation is less prone to noise variations. The UCIR processing approach has an accuracy of 98 cm and 121 when using BMA and BSDA respectively, which is worse than the other approaches. 50% of the time, the objects are estimated by BMA within 5 cm (ACIR) compared to 5 cm for the UCIR and 8 cm for the ICIR. 75% of the time, the objects are estimated within 9, 11 and 19 cm for ACIR, UCIR and ICIR. The targeted application and its requirements are therefore to take into account to determine the data processing method. As mostly robustness is important, further evaluations are discussed on the ACIR data processing technique, unless explicitly mentioned.

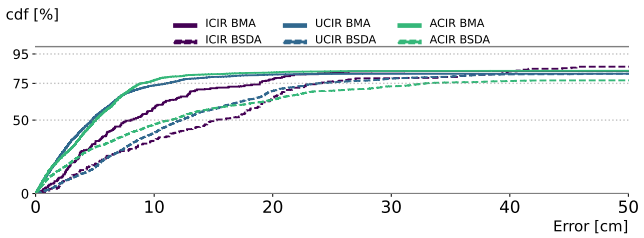

Fig. 7. The cumulative distribution functions when detecting all objects. The ACIR data processing technique is the most robust for object detection. The BMA is on average better than the BSDA distance estimation.

B. Influence of the distance between transmitter and receiver

Next, we determine the impact of the placement of the anchor nodes, e.g. how the distance between the UWB transmitted and receiver impact the detection accuracy.

The results over all objects are given in Fig. 8 in which it becomes clear that the placement of the receiver influences the detection rate. For all objects, the closest receiver has the lowest performance. This can be explained by the positions the objects are placed (on the same y-coordinate as RX1). The best combination of algorithm and receiver is the BMA at receiver 3. The smaller metal box and person are difficult to detect by RX1.

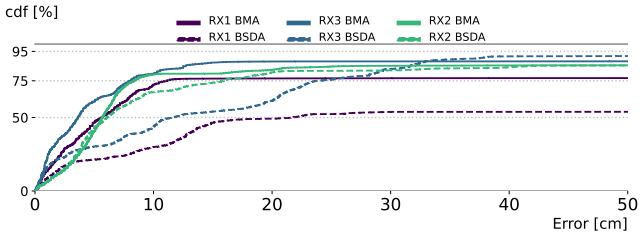

Fig. 8. The position of the receiver influences the distance estimation. RX3 with the largest distance from the tag shows the best performance. The distance between TX and RX are 60 cm (RX1), 120 cm (RX2) and 180 cm (RX3).

C. Impact of the type of obstacle

Four different objects were measured in the IIoT-lab and are detectable with BMA as the CIR has an extra peak when the object is present. Due to space limitations, the maximum distance we can test in our lab is 9 m. The distribution for all objects is given in Fig. 9, while the more detailed errors per distance are given in Table I. For the smaller metal box, we see the performance starts degrading from 5 m (the mean distance error is less than 10 cm up to 5 m), mainly due to bad estimations from RX1. The two bigger metal objects are very well detected. In 95% of the cases, the whiteboard is detected with an error of less than 9 cm. The tv is detected closer than 13 cm for 95% of the cases while 95% of the time the box is detected within 7 cm of its true position. Despite its good percentiles in detection accuracy, the box shows a significantly higher mean error than the other objects (18 cm compared to 5 cm). The person is in half of the cases detected with an accuracy lower than 260 cm. The three metal objects are detected with a mean absolute error (MAE) of 9 cm and 95% of the estimations are within 10 cm. For BSDA For all metallic objects, the distance estimations are worse with BSDA than with BMA.

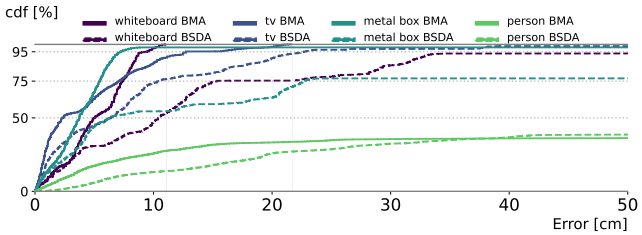

Fig. 9. The whiteboard is the best detected object while the tv and metal box are also detected at dm-level. The person is detected in 33% of the cases within 50 cm.

TABLE I
THE ESTIMATED MEAN ABSOLUTE ERROR WITH THE ACIR DATA PROCESSING AND BMA FOR THE FOUR DIFFERENT TESTED OBJECTS FOR EVERY MEASURED POINT.

Point		120	180	240	300	360	420	480	540	600	660	720	780	840	900
whiteboard	cm	7	6	5	4	5	6	6	6	5	6	4	4	4	5
tv	cm	5	3	3	2	2	4	3	4	2	3	2	15	3	12
metal box	cm	1	4	3	4	4	3	6	12	27	38	40	35	50	18
person	cm	24	8	54	103	115	140	294	414	462	512	532	558	556	628

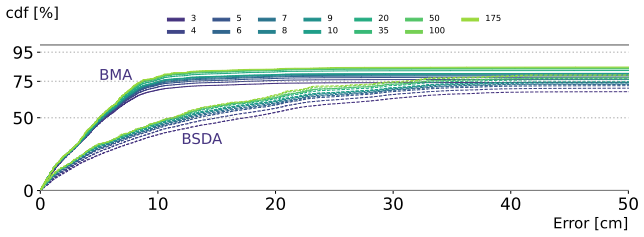

Fig. 10. With an increasing number of CIRs that are used to estimate the distance to the object, the accuracy increases as well. The increase in accuracy when using more than 35 samples (1 second) is limited.

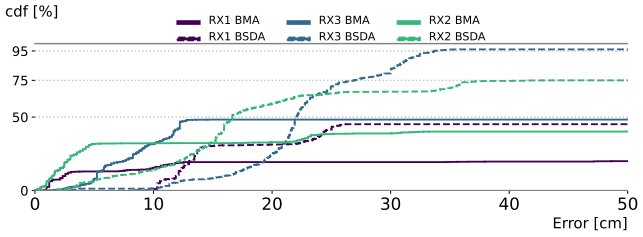

Fig. 11. For the person detection, BSDA at receiver 3 has the highest accuracy. UCIR is used as data processing step and 5 seconds of CIRs were collected.

D. Detection latency

The number of CIRs that are combined gives an indication of the detection time and the responsiveness of the system. The update rate of the current system for data collection is 35 Hz. A higher update rate increases the responsiveness but also increases the time the spectrum is taken and the power consumption. The accuracy to detect objects with a different number of used CIRs is shown in Fig. 10. When collecting more CIRs the error is lower, but the gains of adding more CIRs shows diminishing returns for every additional CIR. When collecting 1 second (35 CIRs) we can detect the object with BMA within 5 cm in 50% of the cases and 9 cm in 75% of the cases. If only 3 CIRs are used, 50% of the cases are detectable within 5.4 cm, but one-quarter of all distance estimations is further than 142.7 cm. The same trends can be observed for the standard deviation variant of the algorithm. Half of the estimations are within 15.5 cm (3 CIRs) or 9.6 cm (35 CIRs) and three-quarters of the points are within 249.8 cm (3 CIRs) or 26.6 cm (35 CIRS). The gains for taking more CIRs in BSDA show a significant improvement at low number of CIRs and smaller improvements in accuracy for more CIRs.

E. Detection of a person

Due to the lower reflectiveness of human bodies, the detection of persons is more difficult than the other obstacles. In contrast to obstacle detection, the best results for person detection are obtained with the ICIR data processing in combination with BSDA distance estimations (MAE: 192 cm). In this case, 50% of the samples are detected within 20 cm of their true position. The UCIR also has the best results with BSDA while ACIR is still better in combination with BMA. When using ICIR preprocessing, the accuracy of the system can be improved by 60 cm when measuring for 5 seconds instead of 1 second. The optimal combination for detecting a person with bi-static radar that we found in the paper is: RX3 with BSDA collecting 5 seconds of data. The results for the three receivers with 175 CIRs are given in Fig. 11. The MAE for ICIR and UCIR are very similar at 44 and 47 cm respectively. For UCIR 95% of the estimations of this receiver are closer than 34 cm and 75% closer than 27 cm. For ICIR, the distribution is different at a lower 75th percentile (22 cm) while the 95th percentile is significantly higher (83 cm).

VI. CONCLUSION AND FUTURE WORK

UWB radar is a promising technology for safety and industry 4.0 applications that require detecting the distance to obstacles or persons. We discussed 3 data processing methods for alignment of the CIR (ICIR, UCIR and ACIR) and 2 detection algorithms (BMA and BSDA). In this study 3 different metal objects are located with UWB radar of which the largest are best detectable. Basic alignment on the integer part (ICIR) of the CIR results has the lowest complexity, but also the lowest accuracy in detecting an object. The ACIR technique provides the best results and is able to detect a whiteboard within 9 cm for 95% of the cases between 1.2 and 9.0 m. For smaller objects, the accuracy depends on the object's location and the reflection paths toward the receiver. Persons can be detected at short distances up to 2.4 m accurately with BMA. In ideal circumstances (when using RX3) we were able to localize the person 95% of the time within 30 cm. The CIR data processing techniques are stable enough to estimate objects correctly within 1 second, often with even lower response times.

The proposed work is an initial step and can be further enhanced with directional antennas. These antennas mitigate undesired reflections from behind, above, and below. In addition, the direct path between the antennas is attenuated with directional antennas which makes reflections more visible in the CIR signal improving the accuracy. A more directed antenna gain at the receiver's node towards the object can increase the maximal distance of UWB radar. Secondly, the algorithms can be expanded to detect multiple objects simultaneously and be scaled toward different environments. To this end, multiple distance peaks can be distinguished while the best algorithm parameters are automatically calibrated. Thirdly, permanent installations should regularly self-learn the background CIR used in the algorithms to limit false positives when environmental parameters change (e.g. temperature, new furniture, ...). Finally, including machine learning for noise removal in the CIR or to detect changes in the CIR compared to the background are worth investigating in more detail.

REFERENCES

[1] A. Karmakar, N. Dey, T. Baral, M. Chowdhury, and M. Rehan, "Industrial internet of things: A review," 03 2019, pp. 1–6.

[2] A. Moschevikin, E. Tsvetkov, A. Alekseev, and A. Sikora, "Investigations on passive channel impulse response of ultra wide band signals for monitoring and safety applications," in *2016 3rd International Symposium on Wireless Systems within the Conferences on Intelligent Data Acquisition and Advanced Computing Systems (IDAACS-SWS)*, Sep. 2016, pp. 97–104.

[3] T. Istomin, E. Leoni, D. Molteni, A. L. Murphy, G. P. Picco, and M. Griva, "Janus: Dual-radio accurate and energy-efficient proximity detection," *PROCEEDINGS OF THE ACM ON INTERACTIVE MOBILE WEARABLE AND UBIQUITOUS TECHNOLOGIES-IMWUT*, vol. 5, no. 4, DEC 2021.

[4] N. Macoir, J. Bauwens, B. Jooris, B. Van Herbruggen, J. Rossey, J. Hoebeke, and E. De Poorter, "Uwb localization with battery-powered wireless backbone for drone-based inventory management," *Sensors*, vol. 19, no. 3, 2019.

[5] M. Aftanas, J. Rovnakova, M. Drutarovsky, and D. Kocur, "Efficient method of toa estimation for through wall imaging by uwb radar," in *2008 IEEE International Conference on Ultra-Wideband*, vol. 2, 2008, pp. 101–104.

[6] S. A. Rane, A. Gaurav, S. Sarkar, J. C. Clement, and H. K. Sardana, "Clutter suppression techniques to detect behind the wall static human using uwb radar," in *2016 IEEE International Conference on Recent Trends in Electronics, Information & Communication Technology (RTEICT)*, May 2016, pp. 1325–1329.

[7] X. Shang, J. Liu, and J. Li, "Multiple object localization and vital sign monitoring using ir-uwb mimo radar," *IEEE Transactions on Aerospace and Electronic Systems*, vol. 56, no. 6, pp. 4437–4450, Dec 2020.

[8] Z. Baird, I. Gunasekara, M. Bolic, and S. Rajan, "Principal component analysis-based occupancy detection with ultra wideband radar," in *2017 IEEE 60th International Midwest Symposium on Circuits and Systems (MWSCAS)*, Aug 2017, pp. 1573–1576.

[9] J. h. Huh and S. h. Cho, "Seat belt reminder system in vehicle using ir-uwb radar," in *2018 International Conference on Network Infrastructure and Digital Content (IC-NIDC)*, 2018, pp. 256–259.

[10] M. Cimdins, S. O. Schmidt, P. Bartmann, and H. Hellbrück, "Exploiting ultra-wideband channel impulse responses for device-free localization," *Sensors*, vol. 22, no. 16, 2022.

[11] C. Li, E. Tanghe, J. Fontaine, L. Martens, J. Romme, G. Singh, E. De Poorter, and W. Joseph, "Multistatic uwb radar-based passive human tracking using cots devices," *IEEE Antennas and Wireless Propagation Letters*, vol. 21, no. 4, pp. 695–699, April 2022.

[12] A. Ledergerber and R. D'Andrea, "A multi-static radar network with ultra-wideband radio-equipped devices," *Sensors*, vol. 20, no. 6, 2020.

[13] B. Van Herbruggen, B. Jooris, J. Rossey, M. Ridolfi, N. Macoir, Q. Van den Brande, S. Lemey, and E. De Poorter, "Wi-pos: A low-cost, open source ultra-wideband (uwb) hardware platform with long range sub-ghz backbone," *Sensors*, vol. 19, no. 7, 2019.

[14] M. Elsanhoury, P. Mäkelä, J. Koljonen, P. Välisuo, A. Shamsuzzoha, T. Mantere, M. Elmusrati, and H. Kuusniemi, "Precision positioning for smart logistics using ultra-wideband technology-based indoor navigation: A review," *IEEE Access*, vol. 10, pp. 44 413–44 445, 2022.

[15] M. Cimdins, S. O. Schmidt, and H. Hellbrück, "Modeling the magnitude and phase of multipath uwb signals for the use in passive localization," in *2019 16th Workshop on Positioning, Navigation and Communications (WPNC)*, 2019, pp. 1–6.

[16] IDLab Ghent University. Industrial iot lab. Accessed: 2022-06-06. [Online]. Available: https://www.ugent.be/ea/idlab/en/research/research-infrastructure/industrial-iot-lab.htm

[17] Decawave, "Dw1000 user manual," Decawave Ltd, Tech. Rep., 2017.